An advanced $TiO_2/Fe_2TiO_5/Fe_2O_3$ triple-heterojunction with enhanced and stable visible-light-driven fenton reaction for the removal of organic pollutants

Yuanxin Deng, Mingyang Xing*, Jinlong Zhang*

Key Laboratory for Advanced Materials and Institute of Fine Chemicals, School of Chemistry & Molecular Engineering, East China University of Science and Technology, 130 Meilong Road, Shanghai 200237, PR China

A B S T R A C T

The construction of catalysts with high efficiency and stability for heterogeneous Photo-Fenton reaction Heterogeneous (PFR) has been a major challenge for the degradation of organic pollutants. Here, we successfully develop an advanced $TiO_2/Fe_2TiO_5/Fe_2O_3$ triple-heterojunction structure by using the mesoporous TiO_2 spheres as the substrate via a simple ion-exchange method. The XRD and HRTEM results demonstrate the generation of Fe_2TiO_5 on the interface between TiO_2 and Fe_2O_3, which can be used as a "bridge" to transfer the photo-excited electrons from TiO_2 to Fe_2O_3. The as-prepared triple-heterojunction has abundant interphase boundaries which greatly improve the migration of photo-excited charges among different components. As a result, the prepared triple-heterojunction has a significantly enhanced PFR activity for the visible-light-driven degradation of methyl orange (MO) and colorless organic pollutant of phenol, compared with the single catalysts of Fe_2O_3 and TiO_2, and the binary-heterojunction of TiO_2/Fe_2O_3. Compared to the traditional Fe_2O_3 based PFR, the degradation rates of MO and phenol over triple-heterojunction can be increased from 4% to 87% within 10 min irradiation and from 38% to 100% within 60 min irradiation, respectively. And the total organic carbon (TOC) degradation rate of phenol can be up to 85%. Moreover, this advanced triple-heterojunction has a wide pH value range of application in PFR. Either at a pH of 4.0 or 7.0, it shows a much higher and more stable PFR activity for the degradation of MO than the catalysts of Fe_2O_3 and TiO_2/Fe_2O_3. And the reaction rate of $TiO_2/Fe_2TiO_5/Fe_2O_3$ almost keeps changeless even after 10th cycles, suggesting its vast application foreground in the environmental pollutant treatment.

© 2017 Elsevier B.V. All rights reserved.

1. Introduction

As one of the most popular advanced oxidation process (AOPs), Fenton reaction has attracted a wide attention for the degradation of organic pollutants in recent years [1–7]. The Fenton reaction can be divided into homogeneous reaction and heterogeneous reaction according to the reaction medium. Homogeneous-Fenton has a very high reaction efficiency for the decomposition of H_2O_2 but cannot be recycle for the continuous reaction, owing to the generation of by-products of iron cements during the degradation of organic pollutants which greatly increase the costing of the reaction [8]. Differently, the heterogeneous-Fenton can realize the catalysts recycle but it always shows a low reaction efficiency, owing to the

low Fe^{3+}/Fe^{2+} cycle efficiency on the catalyst surface [9,10]. And the stability of heterogeneous Fenton reaction is always very poor due to the by-products of iron cements covered on the catalyst surface to cause the poisoning. In order to overcome the low activity of heterogeneous Fenton reagent like Fe_2O_3 for the degradation of organic pollutants, Photo-Fenton reaction (PFR) has been developed to introduce the solar energy to further improve the cycle efficiency of Fe^{3+}/Fe^{2+} in the Fenton reaction.

Recently, Feng et al. [11] used the photoassisted Fenton technology to successfully degrade the ordinary hydrophobic cross-linked polystyrene microspheres and sulfonated cross-linked polystyrene (CS-PS) beads which cannot be degraded by the traditional Fenton reaction. Upon the addition of H_2O_2 and the application of UV irradiation, the photoassisted Fenton reaction on the surface of the CS-PS beads immediately started to disintegrate the polymer matrix of the polystyrene particles. Although they did not give a clear explanation for the mechanism of degrada-

tion of polystyrene materials, they supposed that the generation of Fe(IV) and/or Fe(V) oxo species via the photolysis of some Fe(III) superoxide species was the reason for the degradation of polystyrene. Zhang et al. [12] investigated the UV assistant Fenton processes with two chelating agents, nitrilotriacetic acid (NTA) and [S,S]-ethylenediamine-N,N'-disuccinic acid ([S,S]-EDDS), for the treatment of oil sands process-affected water (OSPW) at natural pH. And their new founding that NTA is a much better chelating agent than EDDS for the application of the UV-Fenton process on the treatment of OSPW at natural pH has a significant impact on the further development of OSPW remediation. In addition to the UV-Fenton, visible-light-assistant Fenton is another effective way for the degradation of organic pollutants. Cai et al. [13] prepared a visible-light-responsive Fenton catalyst of $ZnFe_2O_4$ by a simple reduction-oxidation method. The absorption capability of $ZnFe_2O_4$ in visible-light region was demonstrated by the high rate of Orange II decolorization under Visible/$ZnFe_2O_4$/H_2O_2 Fenton reaction process. The free hydroxyl radical ($\cdot$OH) on the surface of the catalyst was found to be the dominating reactive species for the Orange II removal. Xu et al. [14] employed the sulfate functionalized Fe_2O_3/TiO_2 nanotubes as the visible-light-active heterogeneous photo-Fenton catalysts to degrade the commercial dye reactive brilliant red X-3B. After the sulfate groups were introduced into the structure of Fe_2O_3/TiO_2 nanotubes, the photocatalytic performance was enhanced owing to the enlargement of light absorption and surface acidity. Most recently, Xiao and his co-workers investigated the g-C_3N_4/NH_2-Iron terephthalate metal-organic framework heterojunction for visible-light-induced Fenton-like excitation of H_2O_2 for MB degradation [15]. The excitation of H_2O_2 over the composite is clarified to go through i) the direct and ii) the photo-induced Fenton-like reactions, while the latter is greatly facilitated by the formation of the g-C_3N_4/NH_2-MIL-88B(Fe) heterojunction. As a result, 100% of MB photodegradation was achieved by the heterojunction within 120 min under visible light irradiation, much greater than g-C_3N_4 and NH_2-MIL-88B(Fe), individually. Although a great progress on the PFR has been made in the past years, the PFR activity and stability of heterojunction catalyst are still not high enough to meet the requirements of practical application in the removal of pollutants. The question now is mainly manifested in: i) most of reports focus on the decoloration of dyes and it is really difficult to realize the mineralization of phenol by the PFR; ii) it is not sufficient enough to carry out the cycle test for only 4–5 times under a pH $\approx$ 4 condition, and at least 10 times cycle experiment in the neutral condition presents us more convincing evidence; iii) morphology and crystal structure usually play important roles in improving catalytic properties and activity of PFR, but there is less report on enhancing the PFR activity and stability by the construction of a heterojunction structure with advanced morphology and crystal texture.

Here, we design and prepare an advanced triple-heterojunction of TiO_2/Fe_2TiO_5/Fe_2O_3 by using a facile ion-exchange combined with calcination (IEC) method, which possesses a mesoporous and raspberry-like morphology and a three-phase composite crystal structure. The large size pores (10–30 nm) on the heterojunction provide a passageway for the light absorption and pollutants adsorption. The three-phase composite offers a rich phase interfaces for the migration of photo-excited electrons between different components, which is beneficial to the cycle reaction of Fe^{3+}/Fe^{2+} for the PFR. As a result, the TiO_2/Fe_2TiO_5/Fe_2O_3 has a significantly enhanced PFR activity for the degradation of MO and phenol under visible light irradiation. Importantly, even after 10 times cycle test, the catalyst still remains high PFR activity for the removal of organic pollutants under a neutral condition.

2. Experimental

2.1. Materials

Hydroxypropyl cellulose (HPC) was purchased from Sigma-Aldrich. Titanium butoxide (TBOT), tetraethyl orthosilicate (TEOS), sodium hydroxide (NaOH), hydrogen peroxide (H_2O_2, 30%, w/w) were purchased from Shanghai Lingfeng chemical reagent Co., China and Adamas-beta®. Iron chloride hexahydrate ($FeCl_3\cdot6H_2O$) and hydrochloric acid (HCl) were purchased from Sinopharm chemical reagent Co., China. All of the chemicals used were analytical grade without further purification and ultrapure water was used for all preparation process.

2.2. Synthesis of TiO_2 nanospheres

According to the previously reported method [16,17], the colloidal titania nanospheres were prepared. In a typically synthesis procedure, 0.15 g of HPC was dissolved in 100 mL of ethanol under continuous stirring for 30 min, followed by the addition of 300 μL H_2O and 0.85 mL TBOT. The subsequent mechanical stirring leaded to a white colloid solution system, proving the formation of TiO_2 colloids. After aging for several hours, the colloidal TiO_2 nanospheres were collected by centrifugation (11,000 rpm for 4 min) and washed with ethanol and deionized water for several times until the HPC was removed thoroughly.

2.3. Synthesis of TiO_2/Fe_2TiO_5/Fe_2O_3 heterojunction

The raspberry-like TiO_2/Fe_2TiO_5/Fe_2O_3 (TFF) nanospheres were synthesized by an ion-exchange method. The as-prepared TiO_2 nanospheres were re-dispersed in a 20 mL deionized water and the density was then measured. After adding 1.0 mL 2.5 M NaOH solution, the mixed solution was vigorously stirred for 20 min to result in the adsorption equilibrium of sodium ions. Subsequently sodium-modified TiO_2 nanospheres were obtained by centrifugation and washed with deionized water to remove the excess sodium ions, followed by re-dispersed into a 50 mL aqueous solution with varying concentration of iron chloride hexahydrate. After stirring for 2 h to achieve an ion-exchanged equilibrium, the obtained yellow products were collected by centrifugation, washed thoroughly with ethanol, deionized water for three times (11,000 rpm for 4 min) and dried in vacuum at 60 °C. Finally, the TiO_2/Fe_2TiO_5/Fe_2O_3 powders was obtained by calcination at 600 °C for 2 h under an air atmosphere, in which the molar ratio of Fe/Ti is 0.5%, 1.5%, 5%, 13%, 20%, 50%, respectively. For comparison, Fe_2O_3 loaded with TiO_2 but without sodium ion modification were also prepared by the same method, which was labelled as TiO_2/Fe_2O_3 (TF (20%)).

2.4. Synthesis of SiO_2/Fe_2O_3 heterojunction

According to the typical Stöber method [18], 45 mL ethanol containing 4.5 mL TEOS were injected into the mixture of 28 mL ethanol, 7.5 mL deionized water and 3.5 mL $NH_3\cdot H_2O$, after which the white mixture was stirred continuously at room temperature to complete hydrolysis reaction. Then the sediments were collected by centrifugation and washed with ethanol and deionized water respectively for three times (11,000 rpm for 4 min). A certain amount of obtained SiO_2 nanospheres were re-dispersed into a 50 mL aqueous solution with a certain concentration of iron chloride hexahydrate (the molar ratio of Fe/Si is 20%). Following continuously stirring 2 h, the products were collected by centrifugation and washed with ethanol and deionized water. Finally, drying in vacuum at 60 °C and subsequent calcination at 600 °C

for 2 h under an air atmosphere could afford the SiO$_2$/Fe$_2$O$_3$ (SF) nanospheres.

2.5. Characterization

The morphologies and size of all catalysts were characterized by transmission electron microscopy instrument (TEM, JEM-2100EX), scanning electron microscope (SEM, JEOL JSM-6360 LV) and field emission scanning electron microscopy (FESEM, NOVA NanoSEM450). The Brunauer Emmett Teller (BET) surface area was measured by N$_2$ adsorption at 77 K through a fully automatic surface microporous and physical adsorption instrument (JW-BK222). The optical properties of all catalysts were analyzed through the UV–vis diffuse reflectance (DRS, SHIMADZU UV-2450). PC fluorescence spectrophotometer (SHIMADZU RF-5301) was employed to investigate the PL spectra of catalysts. X-ray diffraction (XRD) patterns were obtained in the range of 5–80° (2θ) using a RigakuD/MAX 2550 diffract meter, which was operated at 40 kV and 100 mA and at the condition of Cu K radiation and λ = 1.5406 Å. An instrument with the Perkin-Elmer PHI 5000C ESCA system was conducted at a condition of Al Kα irradiation to study the X-ray photoelectron spectroscopy of samples. The total organic carbon (TOC) concentration of the filterable degradation agent was investigated by the SHIMADZU TOC-L CPN analyzer.

2.6. Measurement of Photo-Fenton reaction (PFR)

The photo-Fenton performance of all as-prepared samples was investigated by employing 10 mg/L methyl orange (MO) and 10 mg/L phenol as the model pollutant. Briefly, 50 mg TFF, TF, SF, TiO$_2$ or Fe$_2$O$_3$ powders were added into a quartz reactor including 50 mL 10 mg/L MO or phenol aqueous solution, respectively. Before the *PFR*, the pH of the degradation system was modulated to 4.0 with the 0.1 M HCl solution, respectively, and then vigorously stirred in the dark for 45 min to reach the absorption-desorption equilibrium. A 300 W Xe lamp equipped with a wavelength cutoff filters (λ ≥ 420 nm) was used as the visible light source. The *PFR* was initiated by injecting 130 μL H$_2$O$_2$ (30 wt%) and exposing the reactors under visible light irradiation, simultaneously. At each fixed time intervals, 2 mL of reaction solution was collected from the catalytic system, and then the catalyst from the solution was separated by 0.22 μm millipore filter. The instrument of UV–vis diffuse reflectance was used to investigate the concentration variations of MO pollution. A SHIMADZU SPD-M20A high-performance liquid chromatograph (HPLC) was employed to monitor the concentration of phenol in the degradation process. For the cycle photo-Fenton test, after the first degradation, the mixture solution was centrifuged and washed with deionized water for several times to
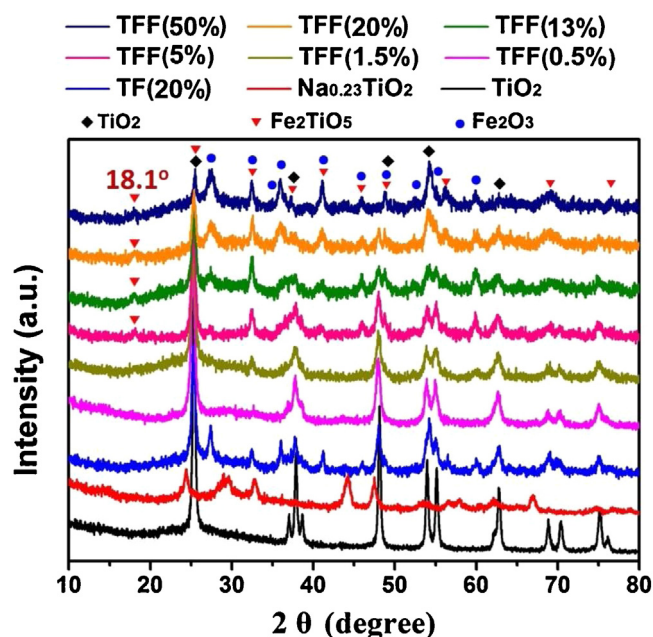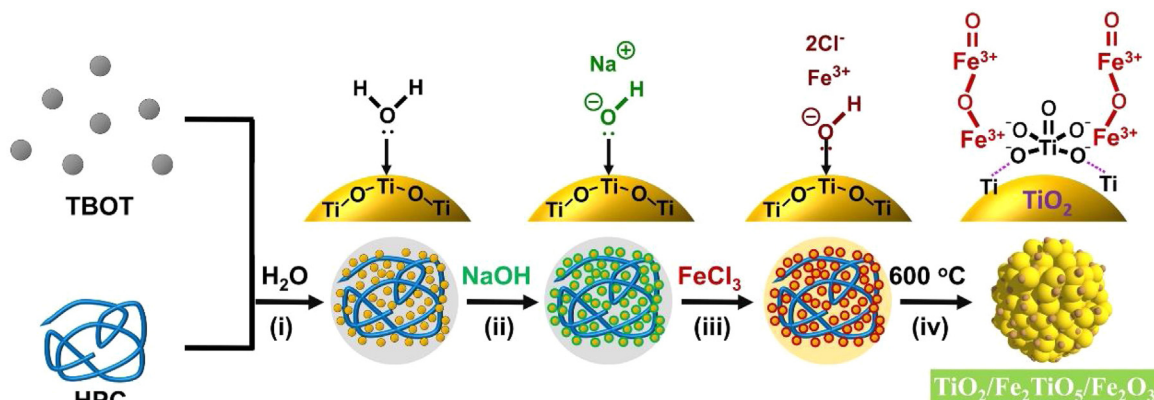

Fig. 1. XRD patterns of TiO$_2$, Na$_{0.23}$TiO$_2$, TF and TFF samples with various loadings (Fe/Ti: 0.5%, 1.5%, 5%, 13%, 20%, 50%).

remove the residual pollutant. After drying in vacuum at 60 °C, the catalysts were recollected for the next Photo-Fenton reaction.

3. Results and discussion

3.1. Morphology and crystal structure

The synthesis schematic of the triple-heterojunction of TiO$_2$/Fe$_2$TiO$_5$/Fe$_2$O$_3$ is shown in Scheme 1. The colloidal titanium oxide spheres are prepared by a homogeneous precipitation method, via using the TBOT as the titanium precursor and using the HPC as the adhesion agent. After that, the NaOH solution was added into the colloidal solution to form the sodium titanate. With the continuous adding of iron chloride hexahydrate solution, the ion-exchange reaction between Fe^{3+} and Na$^+$ is easy to occur on the surface of titanium oxide spheres. A high temperature calcination in the air would result in the crystal transformation of the composite, and three crystal phases could be observed in the products. It is very interesting to obtain the triple-heterojunction of TiO$_2$/Fe$_2$TiO$_5$/Fe$_2$O$_3$ by the combination of ion-exchange and calcination method. Different from the traditional chemical deposition

Scheme 1. Schematic illustration for the formation of raspberry-like triple-heterojunction structure of TiO$_2$/Fe$_2$TiO$_5$/Fe$_2$O$_3$.
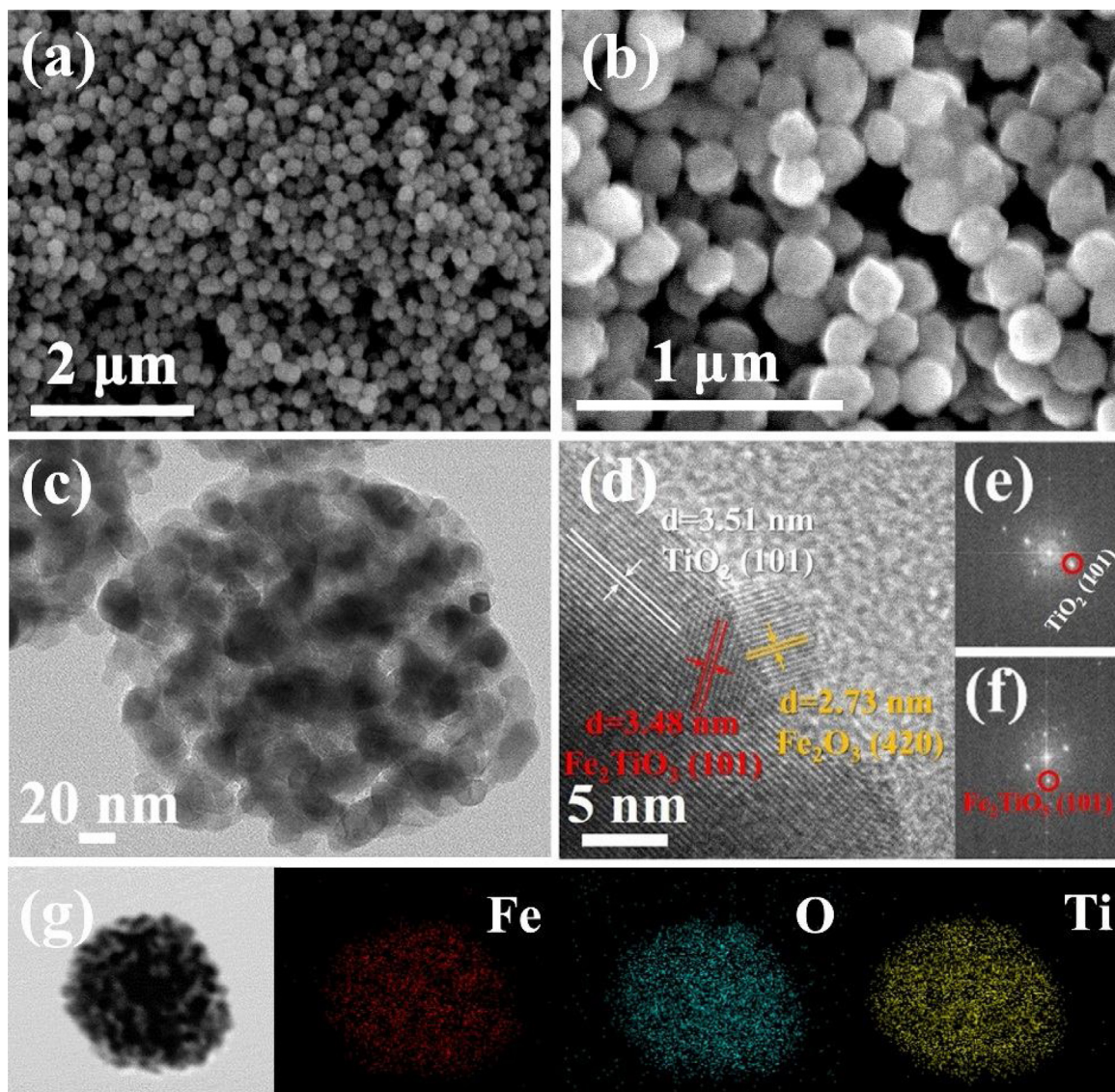
Fig. 2. SEM (a), FESEM (b), and HRTEM (c, d) of TFF(20%); The fast Fourier transform (FFT) patterns on the district of TiO_2 (e) and Fe_2TiO_5 (f); TEM image and the corresponding elemental mapping of Fe, O, and Ti on the TFF(20%) (g).

method for the preparation of heterojunction [19–24], the ion-exchange is a relatively mild method which can achieve the uniform loading of active component on the surface of substrate [25,26]. In addition, according to the Scheme 1, it is not difficult to infer that Fe_2TiO_5 is generated between the TiO_2 and Fe_2O_3, owing to outermost Fe_2TiO_5 is very easy to be transformed into the Fe_2O_3 during the calcination. It must also be mentioned that the conduction band (CB) of Fe_2TiO_5 is located between the CBs of TiO_2 and Fe_2O_3 [27], which is expected to be used as a "bridge" for the transferring of photo-electrons from the TiO_2 to the Fe_2O_3.

The XRD spectra in Fig. 1 represent that the colloidal spheres can be directly transformed into the anatase TiO_2 by a calcination treatment, in the absence of ion exchange procedure. Generally, one of the necessary conditions of the formation of Fe_2TiO_5 involves the effective bonding between Fe(III) species and Ti(IV) atoms in the composition of precursor before calcination, however, which could not be afforded by simply mixing the Fe(III) salt solution with the TiO_2 spheres due to the natural lack of affinity between Fe(III) ions and Ti(IV) atoms. Hence, in this system, the hydroxyl ions are utilized to bridging the two species by ionic bonding with Fe(III) ion and simultaneous coordination with Ti(IV) as shown in Scheme 1.

To introduce the hydroxyl ions, sodium hydroxyl that could totally ionize in aqueous solution is used to modify the TiO_2 spheres followed by the subsequent ion exchange process with Fe(III) ions to afford the $Na_{0.23}TiO_2$ precursor with effective hydroxyl-bridged bonding between Fe(III) species and Ti(IV) atoms. To confirm the necessary role of NaOH, the binary-heterojunction of TF(20%) is prepared by the similar procedure but in the absence of NaOH, and it only shows two phases of TiO_2 and Fe_2O_3 in the XRD spectrum, indicating that the formation of $Na_{0.23}TiO_2$ is very important for the generation of Fe_2TiO_5. To the TFF, with the increasing of $FeCl_3$ amount added in the preparation, there gradually appears a characteristic peak of Fe_2TiO_5 at 18.1°. However, this characteristic peak cannot be observed when the $FeCl_3$ percentage is very low (Fe/Ti: 0.5%–1.5%). There is mainly TiO_2 phase and only small amount of Fe_2O_3 existence in TFF(0.5%) and TFF(1.5%), owing to that only a small number of Fe^{3+} is taking part in the ion exchange reaction.

In order to observe the morphology of heterojunction, SEM and TEM images are shown in Fig. 2, S1, and S2. It is easy to obtain a spherical structure of colloidal titanium oxide by a homogeneous precipitation method (Fig. S1a, b). In the absence of ion exchange, the colloidal spheres can be directly transformed into TiO_2 spheres
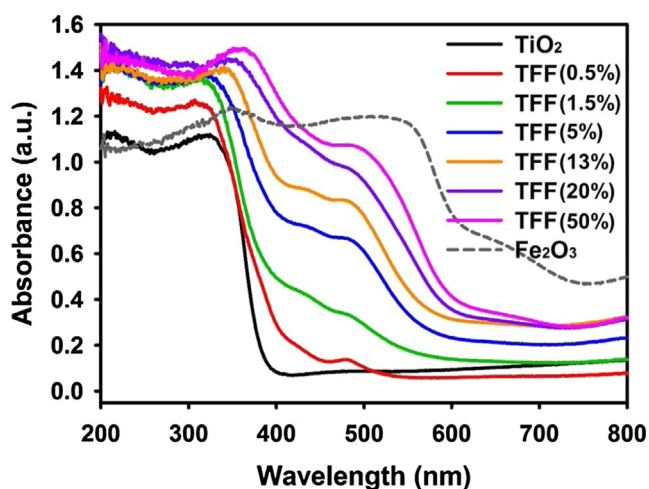
Fig. 3. UV–visible diffuse reflectance spectra of TiO$_2$ and TFFs with various loadings (Fe/Ti: 0.5%, 1.5%, 5%, 13%, 20%, 50%).
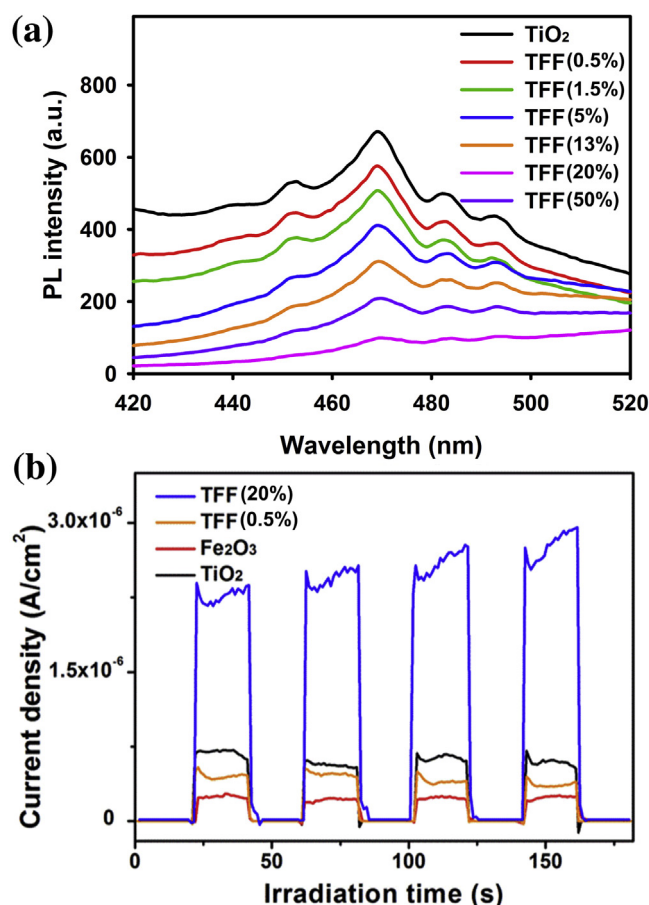

Fig. 4. PL spectra of TiO$_2$ and TFFs with various loadings (excitation wavelength: 365 nm) (a); Transient photocurrent responses of different samples (under visible light irradiation, $\lambda > 420$ nm) (b).

by a calcination treatment (Fig. S1c, d). After the introduction of iron oxides, all of the heterojunctions with different loadings has a similar spherical structure and presents obviously stacked pores (Fig. S2). For instance, the TFF(20%) spheres are highly dispersed and have a uniform diameter of 200 nm, as shown in Fig. 2a and b. The HRTEM image of TFF(20%) shows an obviously porous structure (Fig. 2c), which is formed by the accumulation of nanoparticles. The nitrogen adsorption-desorption isotherm of TFF(20%) indicates that the BET surface area is about 49.2 m^2 g^{-1} and the pore size is mainly in the range of 10–30 nm (Fig. S3), which is consistent with the HRTEM result. These large-sized mesopores are expected to improve the pollutant adsorption and the light multi-reflections in the TFF. According to the measurements of the lattice spacing in Fig. 2d, It can be observed that the lattice fringes are ascribed to the (101) facet of TiO$_2$, (101) facet of Fe$_2$TiO$_5$, and (420) facet of Fe$_2$O$_3$ [28], which have been labeled in Fig. 2d. Interestingly, there is an obvious boundary region between Fe$_2$O$_3$ and TiO$_2$, and the Fe$_2$TiO$_5$ exactly locates on this boundary region to form a triple-heterojunction. The FFT patterns corresponding to the district of TiO$_2$ and Fe$_2$TiO$_5$ are shown in Fig. 2e and f. After carefully calculation on the spots spacing, we can confirm that the spots in Fig. 2e and f are assigned to the (101) facet of TiO$_2$ and the (101) facet of Fe$_2$TiO$_5$, respectively, which is consistent with the HRTEM results. Fig. 2g shows elements mapping for the TFF(20%), which reveals the homogenous distribution of Fe in the triple-heterojunction.

3.2. Optical absorption and charge separation

The UV-DRS spectra of TFF samples with different loadings are shown in Fig. 3. It is unsurprising that all the TFF samples have a significant absorption enhancement in the visible light region, compared with the blank TiO$_2$. With the increasing of the loading of iron oxides, the absorption of TFF has a gradually increasing trend in the visible light. And when the loading amount reaches 50%, the profile of absorption curve of TFF(50%) is close to that of pure Fe$_2$O$_3$, implying that the Fe$_2$O$_3$ loaded on the catalyst surface plays an important role for the visible light absorption. Additionally, the TFFs with a high loading of 5%, 13%, 20% and 50% have a much stronger light adsorption than that of the TFFs with a low loading of 0.5% and 1.5%. Hence, we can deduce that the PFR activity of the TFF with a high loading will be much better than that of the TFF with a low loading. Additionally, all the TFFs have an obviously stronger UV light absorption (200–400 nm) than the TiO$_2$ and Fe$_2$O$_3$, which

may be attributed to the light multi-reflections in the meso-pores to enhance the light absorption.

According to the above discussion of the UV-DRS results, we can conclude that the TFF with a strong visible light adsorption will have an excellent photo-excited charge separation, owing to the high light utilization efficiency and the rich interfaces generated in the TFF. The PL spectra (excitation wavelength is 365 nm) of different samples are shown in Fig. 4a to investigate the charge separation of TFF (corresponding PL spectra excited by 420 nm could be seen in Fig. S4). With the increasing of iron oxides loading, the PL intensity has a distinctly decrease trend. And when the loading amount is 20%, the corresponding TFF displays the lowest PL intensity, which suggests the outstanding efficiency of charge separation on TFF(20%). The TFF(50%) has a higher PL intensity than that of TFF(20%) possibly due to that excessive Fe$_2$O$_3$ covered on the catalyst surface is adverse to the light absorption on the Fe$_2$TiO$_5$ which is mainly seated on the boundary between TiO$_2$ and Fe$_2$O$_3$. In addition to the PL, the photocurrent measurement was also carried out to investigate the charge migration efficiency on TFF, as shown in Fig. 4b. As expected, the TFF(20%) has a much higher visible-light-driven current intensity than other catalysts like TFF(0.5%), TiO$_2$ and Fe$_2$O$_3$, which indicates the excellent charge migration among different components within the triple-heterojunction. The weak current intensity of TFF(0.5%) suggests that the formation of Fe$_2$TiO$_5$ plays a key role for the charge migration in TFF.
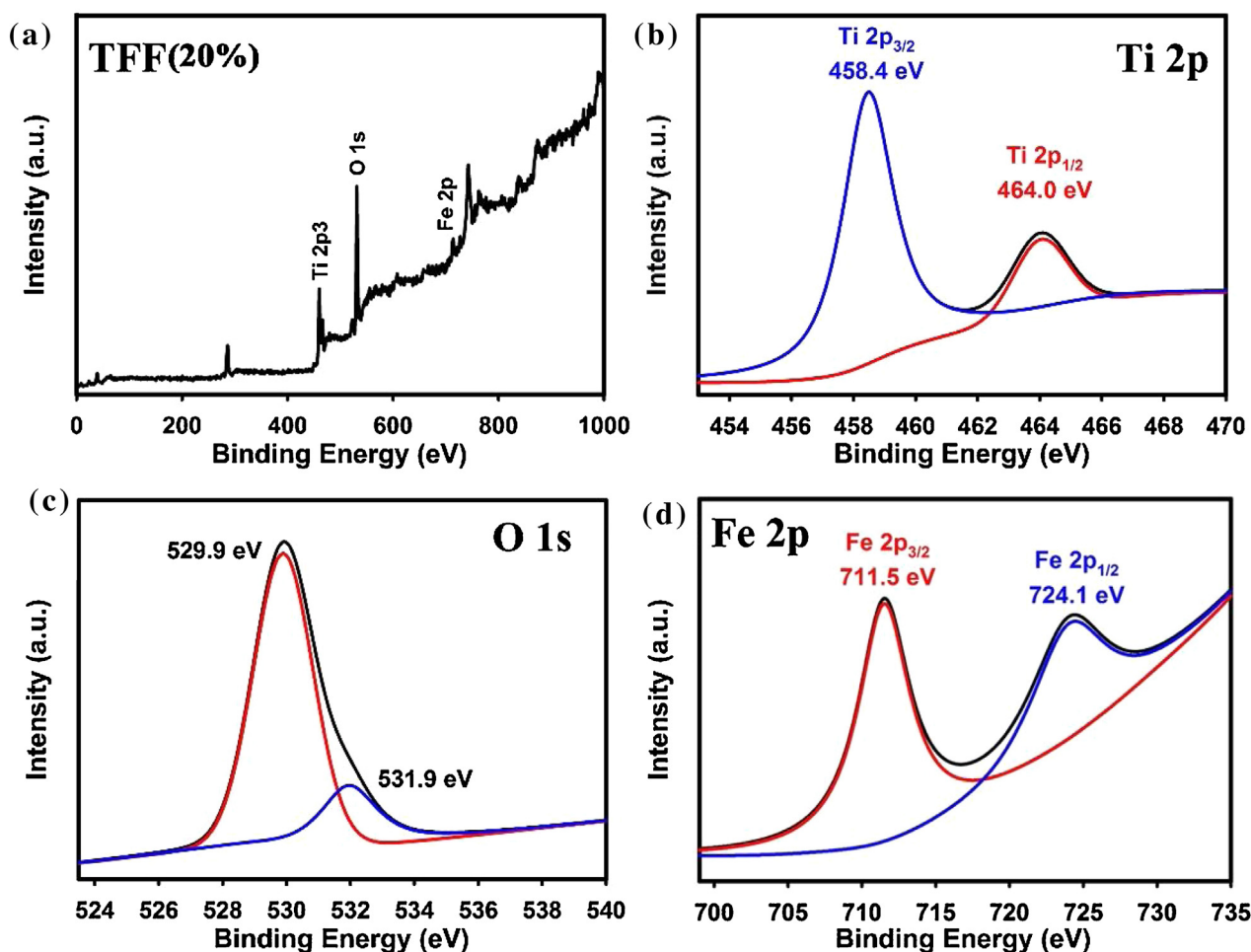
Fig. 5. Full scanned XPS spectrum (a), and Ti 2p (b), O 1s (c), Fe 2p (d) XPS spectra of TFF(20%).

3.3. Chemical composition

The XPS spectra of different elements in TFF are shown in Fig. 5. The full scanned XPS spectrum indicates that the TFF(20%) are mainly composed of three elements of Ti, O and Fe (Fig. 5a). The peaks at 485.4 eV and 464.0 eV in the Ti 2p XPS spectrum of Fig. 5b are ascribed to the characteristic peaks of TiO_2 [29], suggesting the presence of TiO_2 in the triple-heterojunction. Seen from the O 1s XPS spectrum of Fig. 5c, the peak at a low binding energy of 529.9 eV can be assigned to the Ti-O bands in TiO_2 and the Fe-O bonds in iron oxides [30,31]. And another peak at a 531.9 eV implies there are some surface hydroxyl groups connected on the surface of TFF [30]. In order to identify the chemical environment of Fe, Fe 2p XPS spectrum of TFF(20%) is given in Fig. 5d. The peaks at 711.5 eV and 724.1 eV are all attributed to the Fe^{3+} which is mainly existence in Fe_2TiO_5 and Fe_2O_3 [31,32]. The XPS results further confirm that the triple-heterojunction of TFF is constituted of TiO_2, Fe_2TiO_5 and Fe_2O_3.

3.4. Visible-light-driven PFR activity and stability of catalytic performance

We first survey the visible-light-driven PFR performance for the removal of MO under different conditions, as shown in Fig. 6a. It is a matter of course that the activity is extremely poor when there is no light, or no catalyst in the system. Additionally, in the absence of H_2O_2, the activity of TFF for the removal of MO under the visible light irradiation is also very low, indicating that

the occurred catalytic reaction here indeed belongs to the Fenton reaction. It is unsurprised that the activity of TFF in the dark is much lower than that under the light, owing to the absence of photo-charges generated in the dark. In order to investigate the migration of photo-charges between different components in the heterojunction, we have chosen the SiO_2 instead of TiO_2 to prepare the heterojunction of SiO_2/Fe_2O_3 (SF) by using the similar procedure, and its PFR activity for the degradation of MO is shown in Fig. 6b. Compared to TF, the SF has a very low PFR activity, owing to the weak conductivity of SiO_2 which is harmful to the migration of photo-excited electrons from SiO_2 to the iron oxides. The excellent activities of TF and TFF indicate that the TiO_2 is an ideal semiconductor for the transference of photo-excited charges in the heterojunction. Although the TF has a better MO adsorption capacity than the TFF, the activity of TF is worse than that of TFF. Most importantly, the TFF has a much better stability than TF, which will be discussed in detail in the following section. In addition to TiO_2, the Fe_2TiO_5 also plays an important role in the PFR performance. As shown in Fig. 6c, the TFFs with a high loading of iron oxides (Fe/Ti > 5%) have a much better activity than the TFFs with a low loading (<1.5%). According to the XRD results (Fig. 1), when the Fe/Ti percentage is lower than 1.5%, there is no any Fe_2TiO_5 generated in the TFF. The low activities of TFF(0.5%) and TFF(1.5%) are mainly due to the absence of Fe_2TiO_5 and the absence of abundant interfaces which plays an important role in the migration of photo-excited charges between different components (detailed discussion in the following section). Moreover, compared with pure Fe_2O_3, all the TFFs have varying degrees of increase for the MO adsorption in
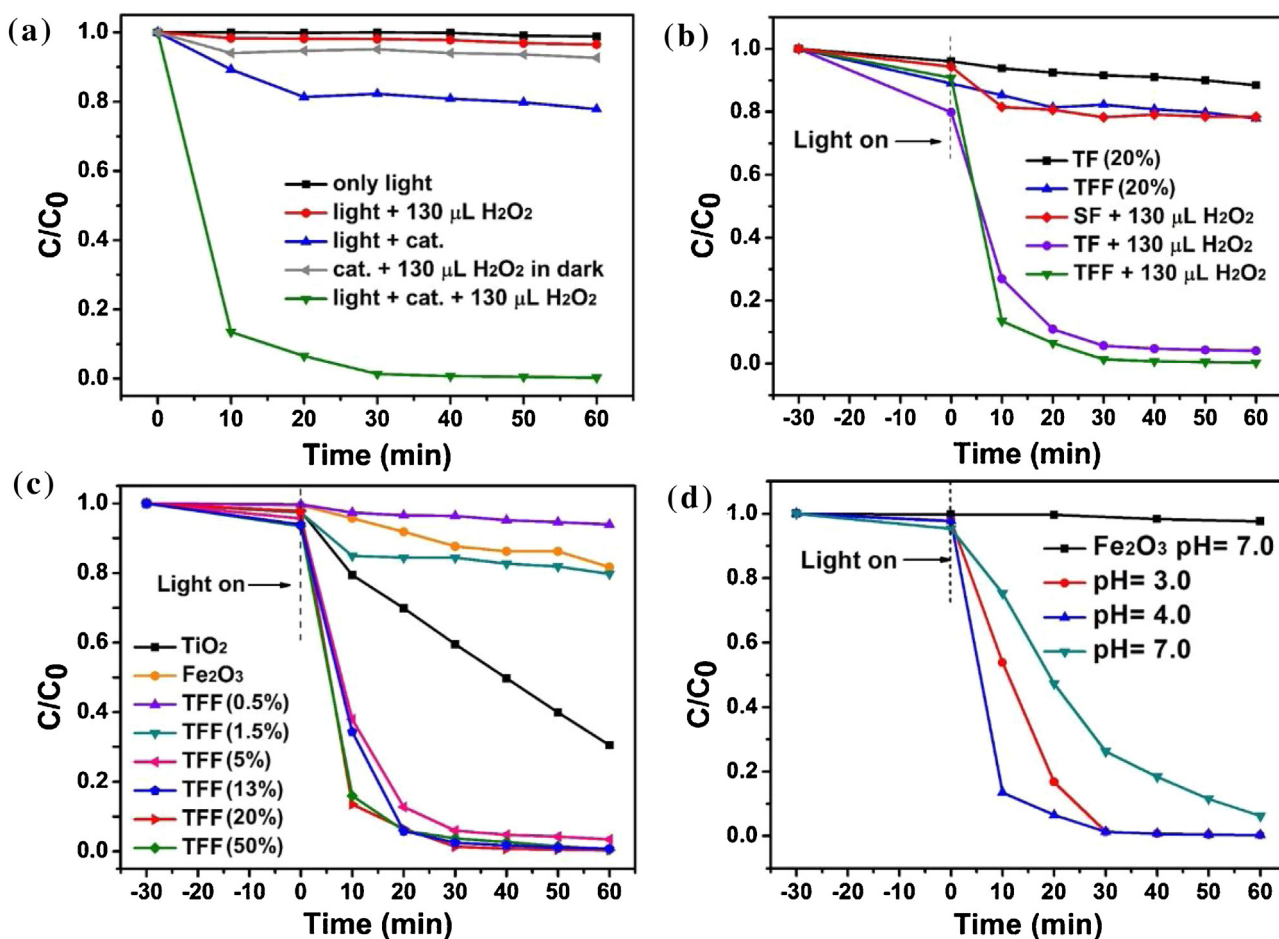
Fig. 6. PFR performance for the degradation of MO under the visible light ($\lambda > 420$ nm; MO: 10 mg L^{-1}; Cat.: 1 mg mL^{-1}; 30 wt% H$_2$O$_2$: 130 μL; the initial pH = 4.0). (a) Comparison of PER activity of TFF(20%) under different conditions. (b) Comparison of adsorption and PFR activity between different catalysts. (c) Comparison of adsorption and PFR activity among the TFFs with different loadings. (d) PFR performance of TFF(20%) under different pH values (pH was adjusted by the addition of 0.1 M HCl solution).

the dark (Fig. 6c), which further confirms the advantage of mesoporous structure. Importantly, the TFF(20%) still has an excellent PFR activity for the degradation of MO even under the neutral condition (Fig. 6d). When the pH value is fixed at 7.0, the degradation rate of TFF(20%) is nearly 95% under the visible light irradiation for 60 min, which is nearly 40 times higher than that of Fe$_2$O$_3$ (2.4%). In addition to MO, the TFF can also degrade the colorless organic pollutant of phenol. Compared to Fe$_2$O$_3$ and TiO$_2$, the TFF(20%) has an significantly high degradation rate for the removal of phenol under the visible light irradiation (Fig. 7). Through the detection of HPLC, the degradation rate of phenol over the TFF(20%) can be up to 100% within 60 min, and the corresponding TOC degradation rate also can achieve to 85% within 120 min irradiation (Fig. S5).

To the Fenton reaction, the stability of catalytic performance for the removal of organic pollutant is one of the most important factors to determine its practical application potential. We have carried out the PFR cycle test of TFF(20%) for the degradation of MO under different pH values. Seen from Fig. 8a, when the pH value was fixed at 4.0, the TFF(20%) shows a very stable PFR activity for the degradation of MO. Even after 10th cycles, its degradation rate keeps almost changeless. Furthermore, the morphology of TFF(20%) is also unchanged after 10th cycles, as shown in the TEM image of Fig. 8b. However, the activity of TF gives an obvious decrease trend after the second cycle test. That means, the presence of Fe$_2$TiO$_5$ in TFF also plays an important role for the enhancing of stability. In order to highlight the stability of TFF, the PFR cycle test under the neutral condition was also carried out, as shown in Fig. 8c.
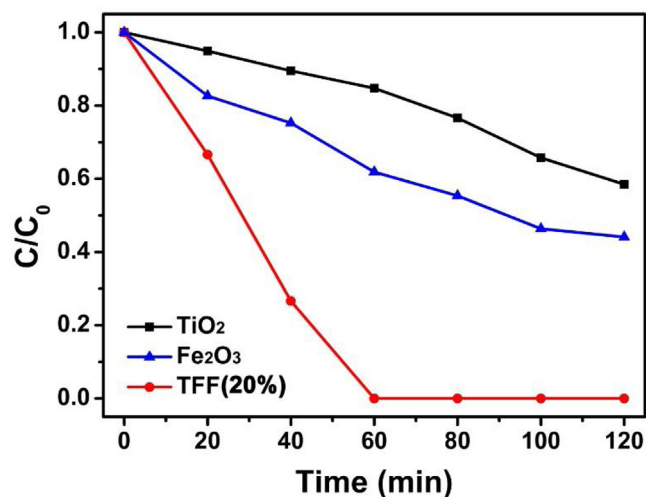

Fig. 7. PFR performance for the degradation of phenol under the visible light ($\lambda > 420$ nm; phenol: 10 mg L^{-1}; Cat.: 1 mg mL^{-1}; 30 wt% H$_2$O$_2$: 130 μL; the initial pH = 4.0).

Compared to Fe$_2$O$_3$, the TFF processes a significantly high and stable activity for the degradation of MO. After second times cycle, the Fe$_2$O$_3$ is close to the inactivation, and however, the TFF still keep the degradation rate of 85% even after 10th cycles. Moreover, the apparent rate constants (Ka) for the PFR of TFF(20%) for the

cycle test is also shown in Fig. 8d. Although the Ka of TFF(20%) has some decrease from 4.65×10^{-2} min^{-1} to 3.19×10^{-2} min^{-1} after 10 times cycle, the absolute value is still much higher than that of Fe$_2$O$_3$ (4.31×10^{-4} min^{-1}). It should be pointed out that the morphology of TFF(20%) also keeps almost changeless after 10 times cycle under a pH $\approx$ 7.0 (Fig. S6), implying the decrease of Ka value in Fig. 8d may be caused by the losing of catalysts during the washing treatment in the cycle test. Hence, compared with the traditional heterogeneous Fenton reaction, we believe the as-prepared TFF catalyst here has a larger potential application for the removal of organic pollutants.

3.5. Mechanism of PFR over TFF

On the basis of the above mentioned experimental results, we can draw a conclusion that the TiO$_2$ and Fe$_2$TiO$_5$ all play very important role in the visible-light-driven PFR for the degradation of organic pollutants. This is mainly manifested in the photo-excited charges migration between different components. The detailed mechanism schematic is shown in Eqs. (1)–(7) and Fig. 9. To the degradation of MO, the MO molecules can absorb visible light to generate electrons which transfer from the LUMO level of MO to the CB of TiO$_2$ (Eq. (1)). These electrons continue to transfer from TiO$_2$ to the CB of Fe$_2$TiO$_5$, owing to the lower CB location of Fe$_2$TiO$_5$. After the stepwise migration, these electrons arrive at the CB of Fe$_2$O$_3$ at last (Fig. 9). Meanwhile, the Fe$_2$TiO$_5$ and Fe$_2$O$_3$ also can absorb the visible light and excite the electrons and holes (Eqs. (2)–(3)), owing to their narrow bandgaps [27]. The holes on the VB of Fe$_2$O$_3$ will transfer to the VB of Fe$_2$TiO$_5$ because of the high VB location of Fe$_2$TiO$_5$ (Fig. 9). As a result, the photo-excited electrons are accumulated at the surface of Fe$_2$O$_3$, and the holes are gathered on the Fe$_2$TiO$_5$. To the degradation of phenol, the mechanism is a little different from the removal of MO. The phenol is one of the most typical organic pollutants, which cannot absorb visible light to generate the electrons. Thereby, most of the photo-electrons come from the Fe$_2$TiO$_2$ and Fe$_2$O$_3$, as shown in Fig. 9. Under the visible light, the electrons are transferring from the CB of Fe$_2$TiO$_5$ to the CB of Fe$_2$O$_3$, and meanwhile, the holes are transferring on the VB of Fe$_2$TiO$_5$. The excellent charge separation improves the lifetime of electrons which can reduce the Fe^{3+} to form the Fe^{2+} on the surface of heterojunction (Eq. (4)). The enhanced Fe^{3+}/Fe^{2+} cycle reaction efficiency on TFF catalyst surface is responsible for the highly efficient PFR degradation of phenol (Eq. (7)).
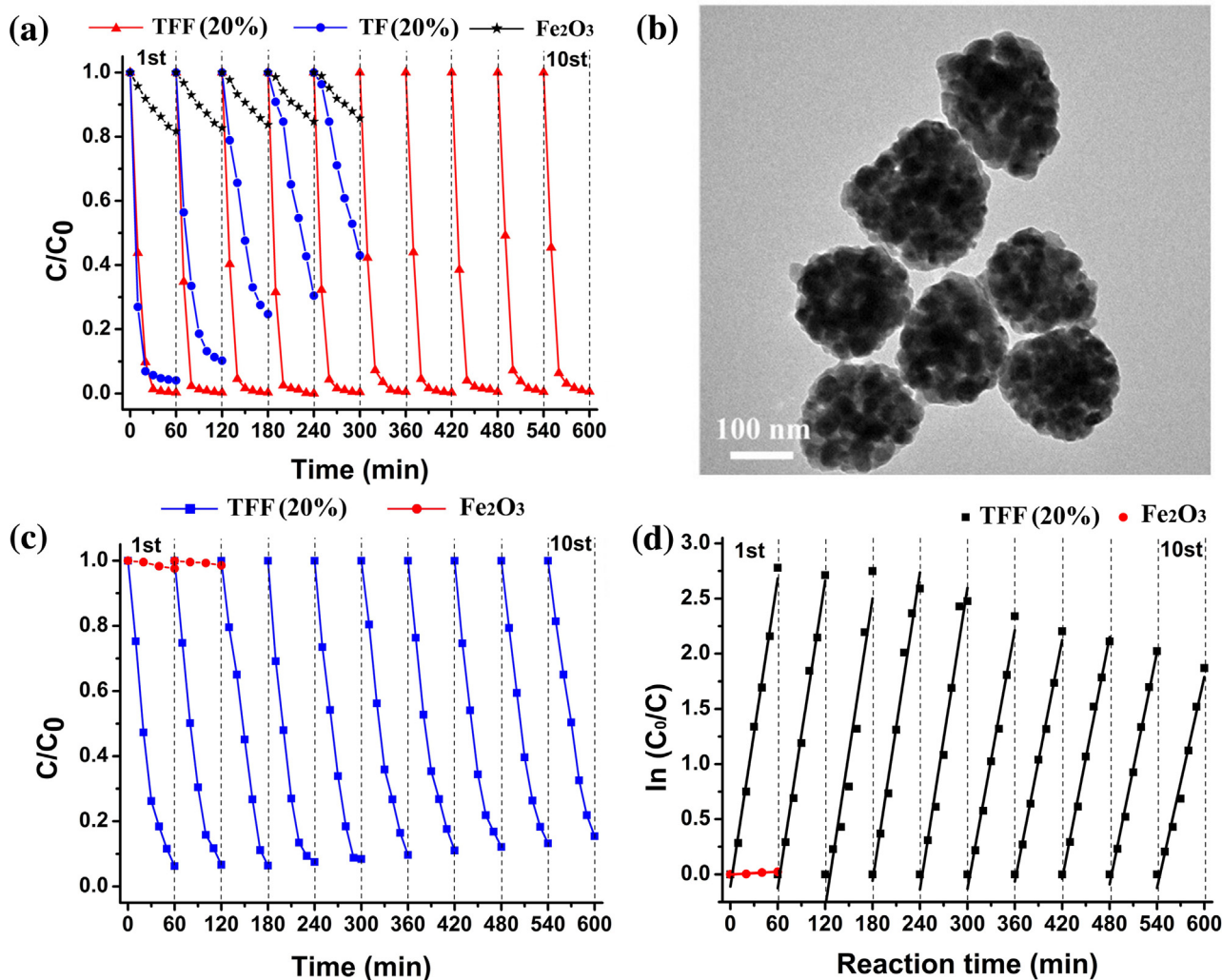
$$Dye \xrightarrow{h\nu} Dye^* + TiO_2(e^-) \qquad (1)$$

Fig. 8. Cycle test for the visible-light-driven PFR over the TFF(20%) for the degradation of MO (λ > 420 nm; MO: 10 mg L^{-1}; Cat.: 1 mg mL^{-1}; 30 wt% H$_2$O$_2$: 130 μL; the initial pH = 4.0) (a), and the corresponding TEM image of the TFF(20%) after 10 times cycle test (b); Cycle test for the visible-light-driven PFR over the TFF(20%) for the degradation of MO at a pH value of 7.0 (c), and the corresponding data of apparent rate constants (Ka) for the cycle test (d).
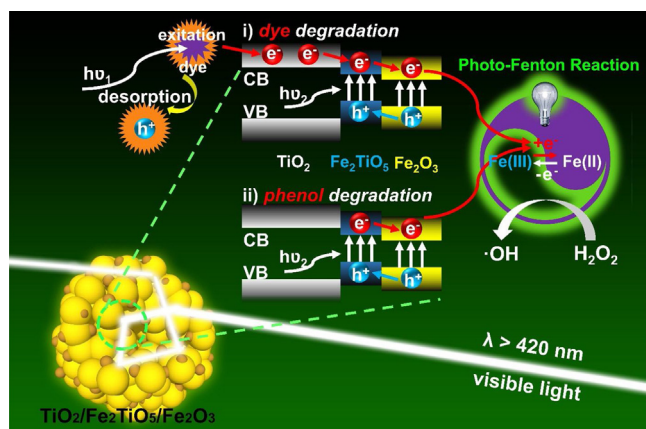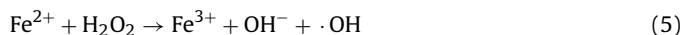
Fig. 9. Visible-light-driven PFR mechanism of $TiO_2/Fe_2TiO_5/Fe_2O_3$ for the removal of different organic pollutants.

$$Fe_2TiO_5 \xrightarrow{h\nu} h^+ + e^- \quad (2)$$

$$Fe_2O_3 \xrightarrow{h\nu} h^+ + e^- \quad (3)$$

$$Fe^{3+} + e^- \rightarrow Fe^{2+} \quad (4)$$

$$Fe^{2+} + H_2O_2 \rightarrow Fe^{3+} + OH^- + \cdot OH \quad (5)$$

$$Dye^* + \cdot OH \rightarrow CO_2 + H_2O \quad (6)$$

$$Phenol + \cdot OH \rightarrow CO_2 + H_2O \quad (7)$$

The PFR is widely considered as a kind of interfacial reaction which is mainly determined by the surface Fe^{3+}/Fe^{2+} cycle reaction. To the TFF, the outer surface of heterojunction is the Fe_2O_3, in which there are a large number of photo-excited electrons which is beneficial to the reduction of Fe^{3+}. The enhancement of the reduction of Fe^{3+} can not only improve the cycle reaction efficiency of Fe^{3+}/Fe^{2+}, but also decrease the losing of iron ions and the generation of iron cements. In other words, there should be less Fe^{2+} ions dissolved from the TFF into the solution. Thereby, we can detect the concentration of Fe^{2+} ions in the aqueous solution by using the 1,10-phenanthroline monohydrate as the probe which can react with the Fe^{2+} ions to show an obvious absorption peak at 511 nm [5], as shown in Fig. 10a. Compared with Fe_2O_3 and TF, the TFF has a much lower peak intensity at 511 nm, indicating the Fe^{3+}/Fe^{2+} cycle reaction is occurring on the catalyst surface rather than in the solution, which is greatly improved by the photo-excited electrons. On the other hand, the TFF in the absence of H_2O_2 shows a very low activity for the degradation of MO as shown in Fig. 6a, indicating that the active groups in the PFR is mainly coming from the decomposition of H_2O_2 rather than the photo-excited holes on the semiconductors. Hence, we have undertaken a detection of $\cdot OH$ in the PFR process by benzoic acid as the probe which can capture the $\cdot OH$ to form the hydroxybenzoic acid with a strong PL signal at about 415 nm, as shown in Fig. 10b. As expected, the TFF(20%) has a higher PL intensity than Fe_2O_3, TiO_2 and TF(20%), which further confirms the advantages of triple-heterojunction structure for the PFR.

4. Conclusions

An advanced $TiO_2/Fe_2TiO_5/Fe_2O_3$ triple-heterojunction has been successfully prepared by a facile IEC method, which shows an excellent PFR activity for the degradation of organic pollutants under the visible light irradiation. Compared to the traditional Fe_2O_3 based and the binary-heterojunction based Fenton reaction, the triple-heterojunction shows some unique advantages in the PFR performance: i) large sized mesoporous structure for the pollutants
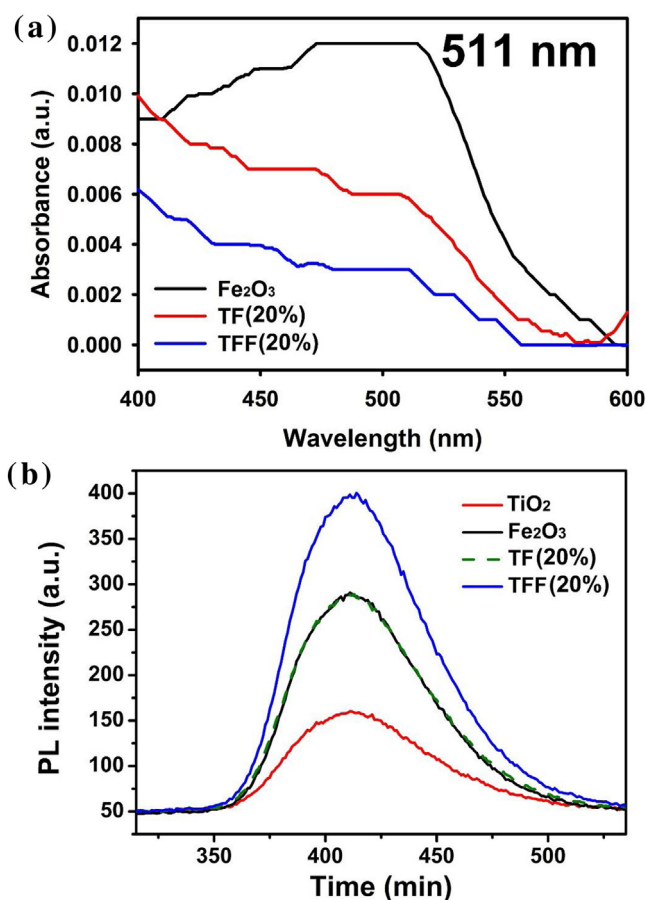

Fig. 10. (a) Absorption spectra of filter liquor, in the presence of catalysts and 1,10-phenanthrolinemonohydrate (the initial pH was 4.0); (b) PL spectra of hydroxybenzoic acid generated under visible light irradiation. (TFF(20%) + H_2O_2 + benzoic acid, at a pH value of 4.0).

adsorption and the light multiple reflection; ii) an excellent visible light absorption owing to the introduction of iron oxides; iii) abundant phase interfaces for enhancing the efficiencies of photo-excited charges migration and separation; iv) high efficiency of Fe^{3+}/Fe^{2+} cycle reaction on the catalyst surface; v) wide pH range of application; vi) stable catalyst structure and PFR performance. The above mentioned advantages determine the much higher and more stable activity of TFFs for the visible-light-driven degradation of MO and phenol than other catalysts of Fe_2O_3, TiO_2 and TiO_2/Fe_2O_3. We believe that our research provides a new strategy for the design and preparation of an effective triple-heterojunction structure for the PFR, which has a large application potential for the removal of organic pollutants.

Author contributions

The manuscript was written through contributions of all authors. All authors have given approval to the final version of the manuscript.

Notes

The authors declare no competing financial interest.

Appendix A. Supplementary data

Supplementary data associated with this article can be found, in the online version, at http://dx.doi.org/10.1016/j.apcatb.2017.04.037.

Additional details of the measurement of $^{\bullet}OH$ and Fe^{2+}, TEM images of catalysts, the nitrogen adsorption-desorption isotherm of catalyst and TOC degradation rate of phenol over the TFF(20%).

References

[1] C. Zhang, W. Bu, D. Ni, S. Zhang, Q. Li, Z. Yao, J. Zhang, H. Yao, Z. Wang, J. Shi, Angew. Chem. Int. Ed. 55 (2016) 2101–2106.
[2] Y. Li, S. Ouyang, H. Xu, X. Wang, Y. Bi, Y. Zhang, J. Ye, J. Am. Chem. Soc. 138 (2016) 13289–13297.
[3] B. Qiu, Y. Deng, M. Du, M. Xing, J. Zhang, Sci. Rep. 6 (2016) 29099.
[4] B. Qiu, Q. Li, B. Shen, M. Xing, J. Zhang, Appl. Catal. B: Environ. 183 (2016) 216–223.
[5] B. Qiu, M. Xing, J. Zhang, J. Mater. Chem. A 3 (2015) 12820–12827.
[6] Z. Ai, L. Lu, J. Li, L. Zhang, J. Qiu, M. Wu, J. Phys. Chem. C 111 (2007) 4087–4093.
[7] X. Huang, X. Hou, J. Zhao, L. Zhang, Appl. Catal. B: Environ. 181 (2016) 127–137.
[8] R.G. Zepp, B.C. Faust, J. Hoigne, Environ. Sci. Technol. 26 (2) (1992) 313–319.
[9] M. Pera-Titus, V. García-Molina, M.A. Baños, J. Giménez, S. Esplugas, Appl. Catal. B: Environ. 47 (2004) 219–256.
[10] X. Hou, X. Huang, Z. Ai, J. Zhao, L. Zhang, J. Hazard. Mater. 310 (2016) 170–178.
[11] H.M. Feng, J.C. Zheng, N.Y. Lei, L. Yu, K.H.-K. Kong, H.Q. Yu, T.C. Lau, M.H.W. Lam, Environ. Sci. Technol. 45 (2011) 744–750.
[12] Y. Zhang, N. Klamerth, P. Chelme-Ayala, M. Gamal EI-Din, Environ. Sci. Technol. 50 (2016) 10535–10544.
[13] C. Cai, Z. Zhang, J. Liu, N. Shan, H. Zhang, D.D. Dionysiou, Appl. Catal. B: Environ. 182 (2016) 456–468.
[14] Z. Xu, C. Huang, L. Wang, X. Pan, L. Qin, X. Guo, G. Zhang, Ind. Eng. Chem. Res. 54 (2015) 4593–4602.
[15] X. Li, Y. Pi, L. Wu, Q. Xia, J. Wu, Z. Li, J. Xiao, Appl. Catal. B: Environ. 202 (2017) 653–663.
[16] Y. Hu, J. Ge, Y. Sun, T. Zhang, Y. Yin, Nano Lett. 7 (2007) 1832–1836.
[17] M. Dahl, S. Dang, J. Bong Joo, Q. Zhang, Y. Yin, CrystEngComm 14 (2012) 7680–7685.
[18] W. Stöber, A. Fink, E. Bohn, J. Colloid Interface Sci. 26 (1968) 62–69.
[19] D. Byun, S. d. Hwang, P.A. Dowben, F.K. Perkins, F. Filips, N.J. Ianno, Appl. Phys. Lett. 64 (1994) 1968–1970.
[20] E.S. Kim, N. Nishimura, G. Magesh, J.Y. Kim, J.W. Jang, H. Jun, J. Kubota, K. Domen, J.S. Lee, J. Am. Chem. Soc. 135 (2013) 5375–5383.
[21] J.A. Love, I. Nagao, Y. Huang, M. Kuik, V. Gupta, C.J. Takacs, J.E. Coughlin, L. Qi, T.S. van der Poll, E.J. Kramer, A.J. Heeger, T.-Q. Nguyen, G.C. Bazan, J. Am. Chem. Soc. 136 (2014) 3597–3606.
[22] W. Zhao, Y. Liu, Z. Wei, S. Yang, H. He, C. Sun, Appl. Catal. B: Environ. 185 (2016) 242–252.
[23] X. Xu, J. Bullock, L.T. Schelhas, E.Z. Stutz, J.J. Fonseca, M. Hettick, V.L. Pool, K.F. Tai, M.F. Toney, X. Fang, A. Javey, L.H. Wong, J.W. Ager, Nano Lett. 16 (2016) 1925–1932.
[24] S. Ning, L. Ding, Z. Lin, Q. Lin, H. Zhang, H. Lin, J. Long, X. Wang, Appl. Catal. B: Environ. 185 (2016) 203–212.
[25] A. Kowalczyk, A. Borcuch, M. Michalik, M. Rutkowska, B. Gil, Z. Sojka, P. Indyka, L. Chmielarz, Microporous Mesoporous Mater. 240 (2017) 9–21.
[26] S. Gupta, S.V. Kershaw, A.L. Rogach, Adv. Mater. 25 (2013) 6923–6944.
[27] E. Courtin, G. Baldinozzi, M.T. Sougrati, L. Stievano, C. Sanchez, C. Laberty-Robert, J. Mater. Chem. A 2 (2014) 6567–6577.
[28] E. Albiter, M.A. Valenzuela, S. Alfaro, G. Valverde-Aguilar, F.M. Martínez-Pallares, J. Saudi Chem. Soc. 19 (2015) 563–573.
[29] X. Chen, L. Liu, Z. Liu, M.A. Marcus, W.-C. Wang, N.A. Oyler, M.E. Grass, B. Mao, P.-A. Glans, P.Y. Yu, J. Guo, S.S. Mao, Sci. Rep. 3 (2013) 1510.
[30] J. Yu, J.C. Yu, W. Ho, Z. Jiang, New J. Chem. 26 (2002) 607–613.
[31] J.Y. Kim, J.-W. Jang, D.H. Youn, G. Magesh, J.S. Lee, Adv. Energy Mater. 4 (2014) 1400476.
[32] S. Gota, E. Guiot, M. Henriot, M. Gautier-Soyer, Phys. Rev. B 60 (1999) 14387–14395.